

## Nanoscale spin polarization in the dilute magnetic semiconductor (In,Mn)Sb

A. Geresdi, A. Halbritter, M. Csontos, Sz. Csonka, and G. Mihály

*Department of Physics, Budapest University of Technology and Economics and Condensed Matter Research Group of the Hungarian Academy of Sciences, 1111 Budapest, Budafoki út 8, Hungary*

T. Wojtowicz

*Institute of Physics, Polish Academy of Sciences, PL-02668 Warsaw, Poland*

X. Liu, B. Jankó, and J. K. Furdyna

*Department of Physics, University of Notre Dame, Notre Dame, Indiana 46556, USA*

(Received 25 March 2008; published 10 June 2008)

Results of point-contact Andreev-reflection experiments on (In,Mn)Sb are presented and analyzed in terms of current models of charge conversion at a superconductor-ferromagnet interface. We investigate the influence of surface transparency, and study the crossover from ballistic to diffusive transport regime as contact size is varied. Application of a Nb tip to a (In,Mn)Sb sample with Curie temperature  $T_C$  of 5.4 K allowed the determination of spin polarization when the ferromagnetic phase-transition temperature is crossed. We find a striking difference between the temperature dependence of the local spin polarization and of the macroscopic magnetization, and demonstrate that nanoscale clusters with magnetization close to the saturated value are present even well above the magnetic phase-transition temperature.

DOI: [10.1103/PhysRevB.77.233304](https://doi.org/10.1103/PhysRevB.77.233304)

PACS number(s): 72.25.Dc, 74.45.+c, 75.50.Pp

Controlling the spin state of electrons provides an important versatility for future electronics.<sup>1</sup> Most of the envisioned spintronic devices are based on spin transfer mechanisms on the nanoscale. For this purpose new materials have been synthesized with highly spin polarized bands, and novel experimental techniques are being applied to characterize the spin state of the charge carriers.<sup>2,3</sup>

(III,Mn)V dilute magnetic semiconductors are promising spintronic materials with high spin polarization<sup>4–6</sup> and with a wide variety of spin-dependent transport properties.<sup>7</sup> While considerable effort is concentrated to enhance the ferromagnetic transition temperature,<sup>8,9</sup> studies of low  $T_C$  alloys are also of great interest, as they contribute to a better understanding of the underlying physics. Here the alloy (In,Mn)Sb—with Curie temperatures below the transition temperatures of conventional superconductors—is especially interesting in that it allows one to study the spin polarization by Andreev spectroscopy *both* in the ferromagnetic and paramagnetic phases.

The Andreev-reflection experiment provides a direct measure of the *current spin polarization*,  $P$ . The current flowing through the interface of a ferromagnet and a superconductor is determined by the charge conversion of individual electrons to Cooper pairs. As a Cooper pair consists of two electrons with opposite spins, the conversion is suppressed in case of spin polarized bands so that  $P$  can be deduced from the voltage dependence of the conductance.  $P$  is often derived in a framework based on the work of Blonder–Tinkham–Klapwijk [denoted by BTK (Ref. 10)], which simply splits the current to unpolarized and fully polarized parts.<sup>3</sup> The net current is then calculated as  $I_{\text{total}} = (1 - P_{\text{BTK}})I_{\text{unpol}} + P_{\text{BTK}}I_{\text{pol}}$  by assuming no Andreev reflection for the fully polarized current and applying the original BTK theory for the unpolarized part. An alternative, more rigorously founded quantification of  $P$ , can be obtained based on the imbalance of spin-dependent transmission coefficients

$P_T = (T_{\uparrow} - T_{\downarrow}) / (T_{\uparrow} + T_{\downarrow})$ .<sup>11,12</sup> Both models assume ballistic transport, but due to the difference in the approaches they cannot be mapped to each other mathematically.

In this Brief Report point-contact Andreev-reflection (PCAR) spectra are presented for (In,Mn)Sb films with ferromagnetic transition temperature of  $T_C = 5.4$  K and for its (In,Be)Sb nonmagnetic counterpart. We analyze the data in terms of the above models for various surface barriers and show that the deduced spin polarizations agree well for the transparent contact limit. We also investigate the crossover from the ballistic to the diffusive transport regime as the contact diameter is varied in a controlled manner. Furthermore the PCAR experiments allow us to compare the temperature dependence of the measured local spin polarization with that of the macroscopic magnetization as the ferromagnetic phase-transition temperature is crossed.

Thin  $\text{In}_{1-x}\text{Mn}_x\text{Sb}$  and  $\text{In}_{1-y}\text{Be}_y\text{Sb}$  film with typical thicknesses of 200 nm were grown by molecular beam epitaxy in a Riber 32 R&D system and were characterized by structural, transport, and magnetic measurements.<sup>13</sup> The hole concentration of these samples is  $n \approx 2 \cdot 10^{20} \text{ cm}^{-3}$ , resulting in a metallic conductivity with  $\sigma \approx 3 \times 10^3 \text{ } \Omega^{-1} \text{ cm}^{-1}$ . In the PCAR experiments mechanically sharpened Nb tips were used as the superconducting electrodes. The position of the tip was regulated by a screw mechanism and a piezoactuator. The accuracy of the positioning is 0.1 nm, as determined from currents measured in the tunneling regime, i.e., before touching the sample surface. In the present study the voltage-dependent differential conductance was acquired using standard four-probe measurements, applying noise filters in the low-temperature stage of the sample holder.

A typical PCAR spectrum is shown in Fig. 1 for (In,Mn)Sb at  $T = 4.2$  K. The bias dependence of the normalized conductance was analyzed in terms of the two models discussed earlier. The best fit obtained with the modified BTK model is shown by the red curve in Fig. 1(a). This

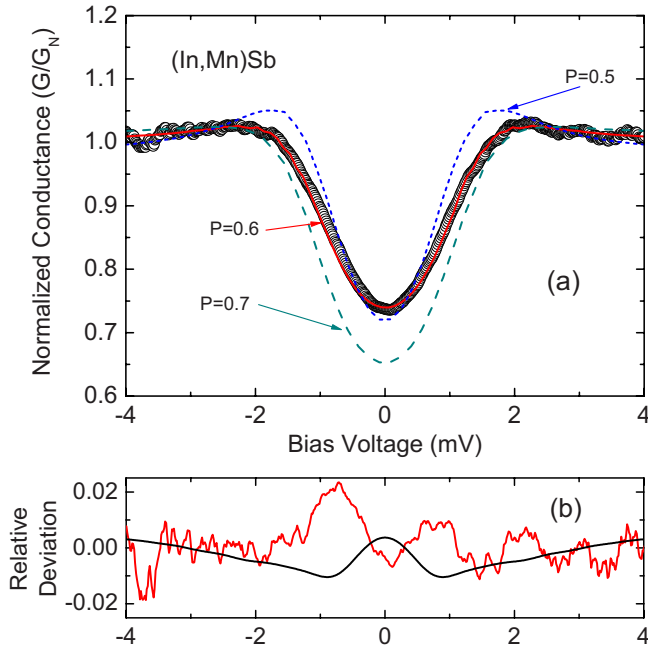


FIG. 1. (Color online) (a) Normalized conductance of a Nb-(In,Mn)Sb contact at  $T=4.2$  K, with fits using the BTK method. The red (gray) solid line with  $P=0.60 \pm 0.01$  yields the best fit (the other fitting parameters are:  $Z=0.13$ ,  $T=4.17$  K, and  $\Delta=1.13$  meV). The dashed lines are fits with intentionally detuned polarizations ( $P=0.5$ ,  $P=0.7$ ) using the same temperature and gap parameters as for the best fit and with  $Z$  as a fitting parameter. (b) Red (gray) curve: deviation of measured data and BTK fitting; black curve: deviation between the two fitting methods as discussed in the text.

represents an almost transparent contact [the  $Z=0.13$  barrier strengths corresponds to  $T=1/(1+Z^2)=0.98$  transmission] and high spin polarization  $P_{\text{BTK}}=0.60 \pm 0.01$ , in good agreement with earlier experimental data.<sup>5</sup> It is to be noted that simulated curves for spin polarization of 0.50 or 0.70 are far away from the measured data, i.e., the value of  $P_{\text{BTK}}$  can really be determined with a high accuracy within this formalism.

Similar high quality fit can also be obtained by calculating the imbalance of spin-dependent transmission coefficients,  $P_T$ .<sup>11,12</sup> There is a small but clear systematic deviation between the two fitting methods, as expected due to differences in the two formalisms [see Fig. 1(b)]. However, the difference between simulations based on the two methods is within the scatter of experimental data and—surprisingly—the fitting parameters for the transmissions  $T_{\uparrow}=0.99$  and  $T_{\downarrow}=0.246$  obtained by this approach correspond to a polarization of  $P_T=0.605$ , which agrees very well with that derived by the BTK theory. A more detailed analysis was carried out by acquiring data using several different contacts. We conclude that, despite the fact that the two models are based on quite different assumptions and cannot be mapped onto each other, they lead to identical results for high quality transparent contacts (denoted by  $Z \rightarrow 0$  and  $T_{\uparrow} \rightarrow 1$ ). For less transparent contacts, i.e., for  $Z > 0.3$ , which correspond to  $T < 0.9$ , the fitting curves obtained using the two methods are still almost identical, but the above excellent agreement in the deduced polarization is lost.

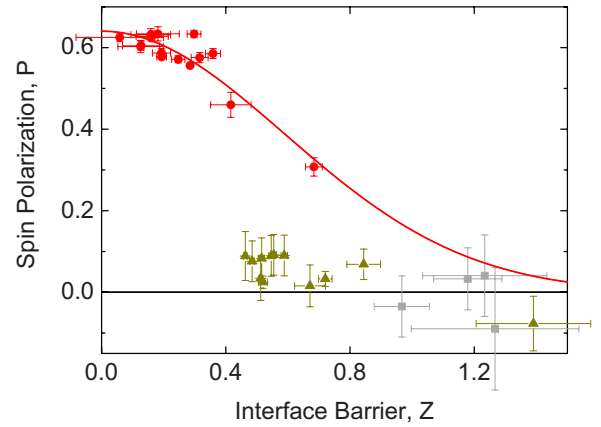


FIG. 2. (Color online) Experimental results for several contacts on the  $P$ - $Z$  plane. Extracted polarization data for Nb-(In,Mn)Sb contacts are denoted by red circles, while the solid red line represents a Gaussian fit based on Ref. 14. Reference data on Nb-(In,Be)Sb and Nb-Au contacts are shown by gray squares and green triangles, respectively.

Next we analyze a large set of PCAR spectra obtained on various contacts at different positions of the sample surface. The results are displayed in the framework of the BTK theory, since this is the method which is generally applied to establish a relation between the parameters characterizing the polarization and the barrier height (transparency). Figure 2 shows the fitting parameters on the  $P$ - $Z$  plane both for the magnetic semiconductor (In,Mn)Sb and for its nonmagnetic counterpart, (In,Be)Sb. Test results on a simple paramagnetic metal (gold) are also shown. The decay of spin polarization with increasing barrier strength observed with Nb-(In,Mn)Sb contacts is attributed to spin-flip scattering in the contact area, and the intrinsic spin polarization of the sample is deduced from fitting the data to a Gaussian shape,<sup>14</sup>  $P(Z \rightarrow 0) = 0.62 \pm 0.01$ . In contrast, the Nb-Au and the Nb-(In,Be)Sb contacts do not exhibit a finite spin polarization, as expected. It is worth noting that the accuracy of the polarization determined from an individual measurement is reduced for high- $Z$  contacts.

The high-accuracy piezopositioning of the Nb tip allows controlled variation of the contact diameter in the range of about 5–50 nm. The Andreev spectra of the magnetic and nonmagnetic samples prepared by the same molecular beam epitaxy technique and having nearly identical bulk parameters<sup>13</sup> are shown in Fig. 3. In these experiments the contact diameter was increased above the literature value of the heavy-hole mean-free path  $l_m \approx 15$  nm, i.e., to the region where diffusive transport is expected. The contact size was estimated from the quasiclassical formula of contact resistance, applicable both to ballistic and diffusive transport,<sup>15</sup>

$$R = (1 + Z^2) \left[ \frac{4\rho l_m}{3\pi d^2} + \gamma \left( \frac{l_m}{d} \right) \frac{\rho}{2d} \right], \quad (1)$$

where  $d$  is the diameter of the contact,  $\rho$  is the bulk resistivity of the material,<sup>13,16</sup> and  $\gamma$  is a prefactor of the order of unity.

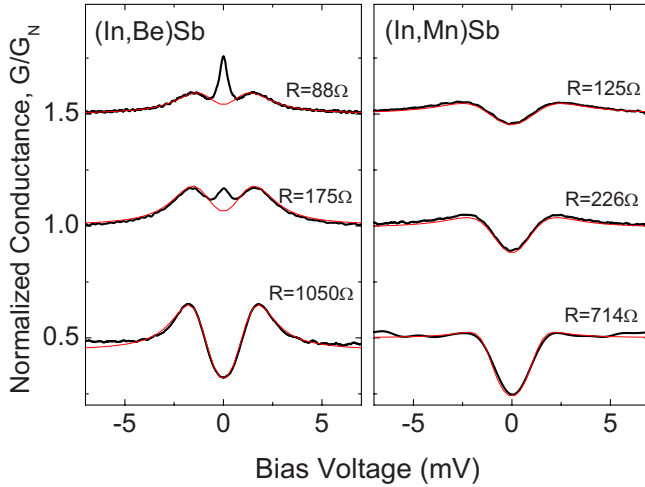


FIG. 3. (Color online) Normalized conductance of several contacts with different contact resistances for nonmagnetic (In,Be)Sb samples (left panel) and magnetic (In,Mn)Sb samples (right panel). The experiments were performed at  $T=4.2$  K. The fits based on modified BTK theory assuming finite lifetime ( $\Gamma > 0$ ) are shown in red (gray). The curves are shifted vertically for clarity.

For large contact areas (small resistances), an unambiguous qualitative feature of diffusive transport is the narrow zero-bias peak observed in the nonmagnetic (In,Be)Sb sample (Fig. 3, left panel). This is attributed to multiple phase-coherent reflections occurring when  $d > l_m$  and the phase-coherence length  $l_\phi > d$ , similarly to the reflectionless tunneling phenomenon observed in superconductor normal metal tunnel junctions.<sup>17,18</sup> In our case the width of the peak is comparable to the thermal energy broadening corresponding to about  $350 \mu\text{V}$  at  $T=4.2$  K. A detailed quantitative description of multiple reflections in diffusive contact regime based on scattering matrix calculations is given elsewhere.<sup>19</sup>

In general, such zero-bias coherence peak is not expected if the Cooper pair conversion occurs in a magnetic sample where the energy of the resulting quasiparticles of opposite spins differs due to the exchange splitting. In that case the phase coherence is lost within a characteristic time determined by this energy difference,  $t_\phi = \hbar / \Delta E_m$ . Indeed, no peak is observable for the Nb-(In,Mn)Sb contact, as shown in the right panel of Fig. 3. Note, however, that a simple mean-field approach for the local magnetic interaction,  $\Delta E_m \approx k_B T_C$ , would mean only a slight broadening of the peak instead of its complete suppression, since in our case  $k_B T_C$  is almost as small as the thermal energy at liquid helium temperature at which the experiment was performed ( $T_C=5.4$  K). Consequently, the absence of the coherence peak implies a much more radical reduction in phase-coherence time, i.e., that the magnetic splitting tested on the length scale of a few nanometer is  $\Delta E_m \gg k_B T_C$ .

Another feature of low-resistance contacts is the smearing of the Andreev spectra on larger voltage scales, both for the magnetic and for nonmagnetic samples. We have found that for contacts with  $d \geq 15$  nm the BTK theory gives unphysical parameters. The fitting temperature obtained by this approach is above the superconducting transition temperature of Nb, while the value of the superconducting gap  $\Delta$  still

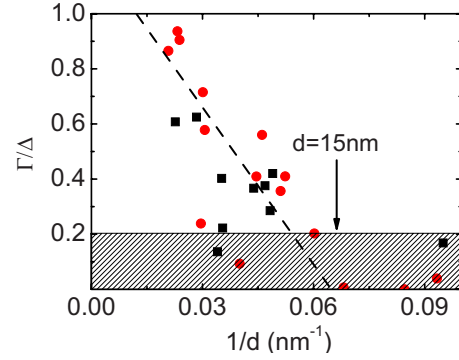


FIG. 4. (Color online) Normalized quasiparticle lifetime parameter as a function of contact size. Red circles and black squares denote data acquired on (In,Mn)Sb and (In,Be)Sb samples, respectively. The onset of finite damping appears at  $d \approx 15$  nm. The dashed line is a guide for the eye.

corresponds to that measured at liquid helium temperature. If, on the other hand, the temperature is fixed at the correct value, the BTK theory gives a rather poor fit. This broadening, however, can be taken into account by introducing a finite quasiparticle lifetime (denoted by  $\Gamma$ ) on the superconductor side.<sup>20</sup> The physical meaning of this phenomenological parameter is the enhanced probability of inelastic scattering in the diffusive regime. Plotting the dimensionless quasiparticle lifetime parameter  $\Gamma/\Delta$  as a function of the contact diameter, we also see that the onset of the diffusive process appears around  $d \approx 15$  nm, as shown in Fig. 4. This feature is independent on whether the sample is magnetic or not: typical fits to data are shown in Fig. 3. We conclude that the smoothing can be attributed to diffusive scattering in the contact area and that it disappears when the contact size is below the mean-free path.

We have also investigated the temperature dependence of the Andreev spectra of (In,Mn)Sb. This study is especially interesting because the use of Nb tip allowed us to cross the ferromagnetic phase-transition temperature. The results are summarized in Fig. 5. Although measurements were taken at temperature far above the Curie temperature of the sample, only thermal broadening is observed, and the dip in the differential conductance denoting local ferromagnetic ordering remains clearly present.

In the analysis of the curves the temperature was used as a fitting parameter, and the values deduced from the measured Andreev spectra agree within 0.1 K with the actual temperature measured independently. One of the most important result of the present study is that *the spin polarization extracted from the fits does not vanish in the paramagnetic phase*. For comparison the remanent magnetization measured by superconducting quantum interference device (SQUID) on the same sample is also shown in Fig. 5.

The above surprising behavior directly confirms the percolation nature of the magnetic phase transition in dilute magnetic semiconductors.<sup>21</sup> The macroscopic magnetization signifies the ordering of magnetic clusters at the Curie temperature, while the local measurement of spin polarization on the 10 nm length scale reveals finite magnetization at temperatures as high as 40% above the phase transition. More-

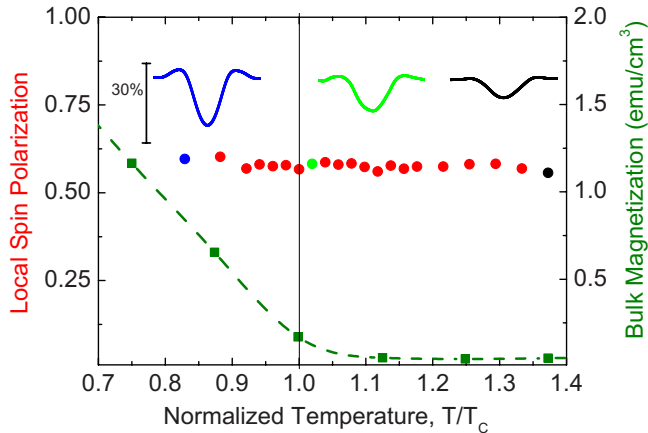


FIG. 5. (Color online) Temperature dependence of the spin polarization acquired from point-contact measurement (circles), and the remanent magnetization determined by SQUID measurement (squares). The PCAR results are reproducible for contacts prepared at various surface positions.

over, the magnetization of the individual clusters does not show any significant change at  $T_C$ , as reflected in the temperature-independent spin polarization. This implies that the characteristic energy scale of cluster formation is much higher than  $k_B T_C$ , in agreement with our earlier analysis of the absence of coherence effects in (In,Mn)Sb. The fact that magnetic clusters with nearly saturated magnetization are present well above  $T_C$  may open the possibility of nanoscale spintronic applications at temperatures far above those required for the *macroscopic* magnetic ordering.

In conclusion, point-contact Andreev-reflection experiments were performed on (In,Mn)Sb and (In,Be)Sb under various circumstances. Results obtained on samples with different surface barriers were analyzed in terms of the extended BTK theory and of the “spin-dependent transmission model,” and it was shown that for the transparent contact limit the two formalisms lead to identical spin polarization:  $P=0.61 \pm 0.01$ . By increasing the contact size in a controlled manner, we were able to enter from the ballistic to the diffusive transport regime, where zero-bias peak due to multiple phase-coherent reflections and smearing of the Andreev spectra were observed. Analyzing the quasiparticle lifetime in (In,Mn)Sb, we found that reliable experiments in the ballistic limit can only be obtained if the contact diameter is less than 15 nm, which corresponds to the heavy-hole mean-free path. The temperature dependence of the spin polarization  $P$  was also investigated, and a striking difference was found between  $P$  and the remanent magnetization. Our observation directly confirms the percolation scheme of the phase transition, with clusters characterized by nearly saturated magnetization even well above the magnetic phase-transition temperature.

This research was supported by the National Science Foundation Grants No. DMR 02-10519 and No. DMR 06-3752, NSF-NIRT Grant No. ECS-0609249, U.S. Department of Energy, Basic Energy Sciences Contract No. W-31-109-ENG-38, and by the Hungarian Scientific Research Fund OTKA under Grants No. NI49881, No. NK72916, and No. F49330. A.H. acknowledges the support from Bolyai János research grant.

- <sup>1</sup>D. D. Awschalom and M. E. Flatte, *Nat. Phys.* **3**, 153 (2007).
- <sup>2</sup>R. J. Soulen, Jr., J. M. Biers, M. S. Ofosky, B. Nadgorny, T. Ambrose, S. F. Cheng, P. R. Broussard, C. T. Tanaka, J. Nowak, J. S. Moodera, A. Barry, and J. M. D. Coey, *Science* **282**, 85 (1998); S. K. Upadhyay, A. Palanisami, R. N. Louie, and R. A. Buhrman, *Phys. Rev. Lett.* **81**, 3247 (1998); Y. Ji, G. J. Strijkers, F. Y. Yang, C. L. Chien, J. M. Byers, A. Anguelouch, G. Xiao, and A. Gupta, *ibid.* **86**, 5585 (2001).
- <sup>3</sup>G. J. Strijkers, Y. Ji, F. Y. Yang, C. L. Chien, and J. M. Byers, *Phys. Rev. B* **63**, 104510 (2001).
- <sup>4</sup>J. G. Braden, J. S. Parker, P. Xiong, S. H. Chun, and N. Samarth, *Phys. Rev. Lett.* **91**, 056602 (2003).
- <sup>5</sup>R. P. Panguluri, B. Nadgorny, T. Wojtowicz, W. L. Lim, X. Liu, and J. K. Furdyna, *Appl. Phys. Lett.* **84**, 4947 (2004).
- <sup>6</sup>R. P. Panguluri, B. Nadgorny, T. Wojtowicz, X. Liu, and J. K. Furdyna, *Appl. Phys. Lett.* **91**, 252502 (2007).
- <sup>7</sup>H. Ohno, *Science* **281**, 951 (1998).
- <sup>8</sup>T. Jungwirth, J. Sinova, J. Masek, J. Kucera, and A. H. MacDonald, *Rev. Mod. Phys.* **78**, 809 (2006).
- <sup>9</sup>M. Jamet, A. Barski, T. Devillers, V. Poydenot, R. Dujardin, P. Bayle-Guillemaud, J. Rothman, E. Bellet-Amarlic, A. Marty, J. Cibert, R. Mattana, and S. Tatarenko, *Nat. Mater.* **5**, 653 (2006).
- <sup>10</sup>G. E. Blonder, M. Tinkham, and T. M. Klapwijk, *Phys. Rev. B* **25**, 4515 (1982).
- <sup>11</sup>J. C. Cuevas, A. Martín-Rodero, and A. L. Yeyati, *Phys. Rev. B* **54**, 7366 (1996).
- <sup>12</sup>F. Pérez-Willard, J. C. Cuevas, C. Sürgers, P. Pfundstein, J. Kopu, M. Eschrig, and H. v. Löhneysen, *Phys. Rev. B* **69**, 140502(R) (2004).
- <sup>13</sup>T. Wojtowicz, W. L. Kim, X. Liu, G. Cywiński, M. Kutrowski, L. V. Titova, K. Yee, M. Dobrowolska, J. K. Furdyna, K. M. Yu, W. Walukiewicz, G. B. Kim, M. Cheon, X. Cheon, S. M. Wang, H. Luo, I. Vurgaftman, and J. R. Meyer, *Physica E (Amsterdam)* **20**, 325 (2004).
- <sup>14</sup>C. H. Kant, O. Kurnosikov, A. T. Filip, P. LeClair, H. J. M. Swagten, and W. J. M. de Jonge, *Phys. Rev. B* **66**, 212403 (2002).
- <sup>15</sup>B. Nikolic and P. B. Allen, *Phys. Rev. B* **60**, 3963 (1999).
- <sup>16</sup>I. Vurgaftman, J. R. Meyer, and L. R. Ram-Mohan, *J. Appl. Phys.* **89**, 5815 (2001).
- <sup>17</sup>A. Kastalsky, A. W. Kleinsasser, L. H. Greene, R. Bhat, F. P. Milliken, and J. P. Harbison, *Phys. Rev. Lett.* **67**, 3026 (1991).
- <sup>18</sup>C. W. J. Beenakker, *Rev. Mod. Phys.* **69**, 731 (1997).
- <sup>19</sup>A. Geresdi, A. Halbritter, and G. Mihály (unpublished).
- <sup>20</sup>A. Plecenik, M. Grajcar, S. Benacka, P. Seidel, and A. Pfuch, *Phys. Rev. B* **49**, 10016 (1994).
- <sup>21</sup>A. H. MacDonald, P. Schiffer, and N. Samarth, *Nat. Mater.* **4**, 195 (2005).